How to cite: *Angew. Chem. Int. Ed.* **2024**, *63*, e202405780
doi.org/10.1002/anie.202405780

C-H functionalization

Cobalt-Mediated Photochemical C–H Arylation of Pyrroles

Julia Märsch, Sebastian Reiter, Thomas Rittner, Rafael E. Rodriguez-Lugo, Maximilian Whitfield, Daniel J. Scott, Roger Jan Kutta, Patrick Nuernberger, Regina de Vivie-Riedle,* and Robert Wolf**

Abstract: Precious metal complexes remain ubiquitous in photoredox catalysis (PRC) despite concerted efforts to find more earth-abundant catalysts and replacements based on 3d metals in particular. Most otherwise plausible 3d metal complexes are assumed to be unsuitable due to short-lived excited states, which has led researchers to prioritize the pursuit of longer excited-state lifetimes through careful molecular design. However, we report herein that the C–H arylation of pyrroles and related substrates (which are benchmark reactions for assessing the efficacy of photoredox catalysts) can be achieved using a simple and readily accessible octahedral bis(diiminopyridine) cobalt complex, **[1-Co]**$(PF_6)_2$. Notably, **[1-Co]**$^{2+}$ efficiently functionalizes both chloro- and bromoarene substrates despite the short excited-state lifetime of the key photoexcited intermediate ***[1-Co]**$^{2+}$ (8 ps). We present herein the scope of this C–H arylation protocol and provide mechanistic insights derived from detailed spectroscopic and computational studies. These indicate that, despite its transient existence, reduction of ***[1-Co]**$^{2+}$ is facilitated via pre-assembly with the NEt_3 reductant, highlighting an alternative strategy for the future development of 3d metal-catalyzed PRC.

Introduction

Photoredox catalysis (PRC) is a relatively new but highly versatile technique that is becoming pervasive in organic synthesis.[1–4] While exact mechanisms can differ, all PRC processes involve single electron transfer to or from an excited state of the photocatalyst **PC** as a key step. The former option involves an electron transfer from a substrate to the excited state of the **PC** (Figure 1a), a process that is often termed "reductive quenching". Since its inception, PRC has relied heavily on second and third row transition metal complexes as **PC**, and especially complexes of the precious metals Ru and Ir.[5,6] Even though they remain probably the most frequently and widely-used family of catalysts for PRC, there are growing concerns around cost, scarcity, and security of supply. This has prompted extensive efforts to find alternative **PC** based on more earth-abundant elements.[7–20] Significant progress has been made in the use of organic dyes as **PC**;[5,6] however it has been argued that this approach is limited by the synthetic complexity of many organic **PC**, and corresponding difficulties in tuning their redox and other catalytically-relevant properties.[19]

In this context, an alternative solution would be to replace the currently employed Ru and Ir polypyridyl complexes with analogues based on their much cheaper 3d metal homologues Fe and Co. However, with a few notable exceptions (e.g. based on Cu^{I})[21–23] 3d metal **PC** remain significantly underdeveloped relative to their precious metal and organic counterparts. This can be attributed to the fact that, in practice, the photophysical and photochemical properties of 3d metal complexes tend to differ fundamentally from those of analogous 4d and 5d complexes.[12,14–19] In particular, for 3d complexes the prevailing excited states ***PC** are typically short-lived, with lifetimes in the fs to ps range.[10,15,24] It has often been argued that these are too short to permit diffusion-limited, intermolecular interactions with

[*] J. Märsch, R. E. Rodriguez-Lugo, D. J. Scott, R. Wolf
Institute of Inorganic Chemistry
University of Regensburg
93040 Regensburg (Germany)
E-mail: robert.wolf@ur.de

S. Reiter, M. Whitfield, R. de Vivie-Riedle
Department of Chemistry
Ludwig Maximilian University Munich
81377 Munich (Germany)
E-mail: Regina.de_Vivie@cup.uni-muenchen.de

T. Rittner, R. J. Kutta, P. Nuernberger
Institute of Physical and Theoretical Chemistry
University of Regensburg
93040 Regensburg (Germany)
E-mail: patrick.nuernberger@ur.de

R. E. Rodriguez-Lugo
present address: Istituto di Chimica dei Composti Organometallici
Consiglio Nazionale delle Ricerche
Via Madonna del Piano 10
Sesto Fiorentino 50019 (Italy)

D. J. Scott
present address: Department of Chemistry
University of Bath
Claverton Down
Bath, BA2 7AY (United Kingdom)

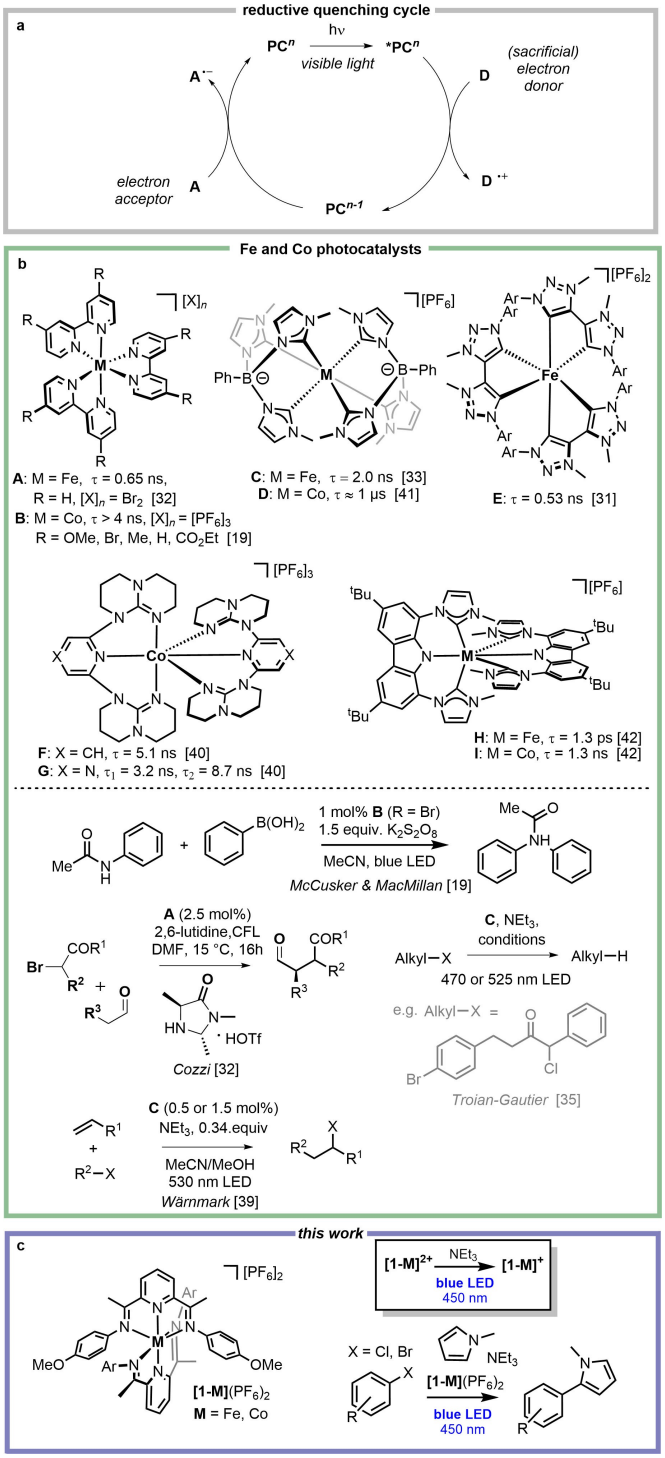

Figure 1. (a) General mechanism of photoredox catalysis mediated by an electron transfer from a sacrificial electron donor (PC = photocatalyst, D = electron donor, A = electron acceptor); (b) previously reported Fe- and Co-based photocatalysts and their catalytic applications; (c) use of simple diiminopyridine complexes as photocatalysts in C–H arylations, as reported herein.

substrates,[12,25] and that this precludes these complexes from being effective **PC**.

This has led to significant efforts to develop Fe and Co complexes with longer ***PC** excited-state lifetimes, and in recent years a number of breakthroughs have been achieved through sophisticated ligand design. Employed strategies include exploitation of the Marcus inverted region,[19] and the destabilization of metal-centered (MC) electronic states with simultaneous stabilization of metal-to-ligand (MLCT) or ligand-to-metal (LMCT) charge transfer states. This could be achieved through the incorporation of push-pull ligand sets, strong π-acceptor ligands, σ-donating *N*-heterocyclic carbenes (NHC) and by σ- and π-donation of cyclometalating ligands.[12,13,26–29] As a result, complexes with excited-state lifetimes well into the ns range have emerged (Figure 1b, top). At the same time, there have been significant advances in electronic structure and dynamics methods,[11,30] enabling a detailed theoretical description of photocatalytic processes.

These fundamental developments have been accompanied by pioneering reports describing early examples of PRC using Fe and Co photocatalysts, some relevant examples of which are shown in Figure 1b.[19,27,31–42] While these reports represent an important advance for the field of PRC, in many cases achieving these longer excited-state lifetimes demand elaborate ligand syntheses, and/or places significant restrictions on molecular design that need to be balanced with the optimization of other important properties such as ***PC** redox potentials. In contrast, we report in this work successful PRC via a simple Co complex with an extremely short excited-state lifetime, demonstrating that long ***PC** lifetimes are in fact not a strict requirement. Specifically, we show that the simple, octahedral, bis(diiminopyridine) cobalt complex **[1-Co]**$(PF_6)_2$[43] successfully mediates the C–H arylation of pyrrole with bromo- and chloroarenes (Figure 1c). Spectroscopic studies confirm the key photochemical reduction of **[1-Co]**$^{2+}$ to **[1-Co]**$^{+}$. High-level quantum chemical calculations reveal the crucial role of preassembly in enabling this process and provide detailed mechanistic insights.

Results and Discussion

Despite the previous emphasis on excited-state lifetimes, we were motivated to investigate whether PRC might in fact be achievable using 3d-based **PC** even with very short-lived ***PC** states. We were encouraged by recent reports from elsewhere in the field of PRC, specifically consecutive photoinduced electron transfer (conPET) and electro-mediated photoredox catalysis (e-PRC) reactions,[44–48] in which intramolecular electron transfer to the excited states of organic radical anions **PC**$^{\bullet-}$ (or from the excited states of organic radical cations **PC**$^{\bullet+}$) has been proposed to be a viable and essential mechanistic step despite the short excited-state lifetimes of these ***PC**$^{\bullet-}$ (or ***PC**$^{\bullet+}$) states.[49–52] As a proof of principle we therefore chose to investigate the catalytic behavior of the known complexes **[1-M]**$^{2+}$ (M=Fe, Co) whose full structures are shown in Figure 1c. **[1-M]**$(PF_6)_2$ are easily synthesized, are based upon a highly tunable ligand scaffold, and their redox properties have

previously been studied in detail being appropriate for PRC.[43]

Photoreduction of [1-Co](PF$_6$)$_2$ by NEt$_3$

The cobalt complex **[1-Co]**(PF$_6$)$_2$ was investigated by transient absorption spectroscopy, which, as expected, showed a short excited-state lifetime of just 8 ps upon excitation at 405 nm (see Figure S44, SI). Nevertheless, the photochemical reduction of **[1-Co]**(PF$_6$)$_2$ by the common sacrificial electron donor NEt$_3$ (Figure 2a) was monitored by electronic absorption spectroscopy in the UV/Vis-NIR spectral range. Irradiation at 405 nm of a solution of **[1-Co]**(PF$_6$)$_2$ (20 μM) and NEt$_3$ (200 μM, 10 equiv. with respect to **[1-Co]**(PF$_6$)$_2$) in MeCN (250 μL) induced clear absorption changes (Figure 2a). The one-electron reduced complex **[1-Co]**$^+$ (Figure 2b) was identified as the reaction product by its characteristic absorption at 340 nm and a broad band extending from 630 nm far into the NIR (see Figure S41, SI).[43] Isosbestic points at 365 nm and 624 nm corroborate direct reduction of **[1-Co]**$^{2+}$ to **[1-Co]**$^+$ and decomposition of the spectra into the individual contributions of both oxidation states (Figure 2a, inset) yields concentration profiles that can be described by the rate equation for a single photochemical step (Figure 2a, see fit in the inset).[53] Since both light and NEt$_3$ are necessary to enable reduction of **[1-Co]**$^{2+}$ (Figures S31–S33, SI), **[1-Co]**$^{2+}$ is reduced in its excited state, ***[1-Co]**$^{2+}$, by NEt$_3$ yielding **[1-Co]**$^+$ and the [NEt$_3$]$^{+\bullet}$ radical cation. The latter cannot be detected because it is rapidly deprotonated due to excess of NEt$_3$ resulting in the formation of products that do not absorb in the spectral detection window (Figure 2b).[54]

The photochemical reduction of **[1-Fe]**(PF$_6$)$_2$ by NEt$_3$ was also investigated showing a significantly reduced efficiency (see Figure S19, SI). This is presumably a consequence of the more negative reduction potential of **[1-Fe]**(PF$_6$)$_2$, influenced by the electronic structure of the reduced complex **[1-Fe]**$^+$, which retains a formal Fe^{II} oxidation state by reducing one of its diiminopyridine ligands to the radical anion (see Figure S47, SI).[43] Furthermore, **[1-Fe]**$^+$ is prone to disproportionation into **[1-Fe]**(PF$_6$)$_2$ and **[1-Fe]**^{0}, as also evident by a non-clean formation of **[1-Fe]**(PF$_6$), even after several days of irradiation.

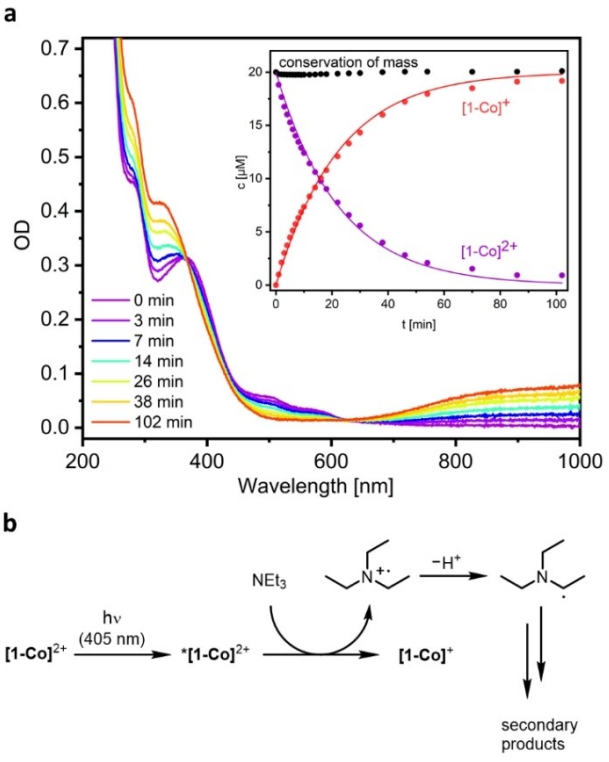

Figure 2. (a) Electronic absorption spectra in the UV/Vis-NIR spectral range of a mixture of **[1-Co]**(PF$_6$)$_2$ (20 μM) and NEt$_3$ (200 μM) in MeCN (250 μL) after different time intervals of irradiation at 405 nm. Inset: Concentration time profiles of **[1-Co]**$^{2+}$ (violet), **[1-Co]**$^+$ (red), and the sum of both profiles demonstrating the conservation of mass (black). (b) Reaction sequence of the photoreduction.

Preassemblies between [1-Co](PF$_6$)$_2$ and NEt$_3$

Due to the extremely short excited-state lifetime of ***[1-Co]**$^{2+}$ a diffusion-limited reaction between this excited state and NEt$_3$ at the concentrations employed experimentally seems unlikely. Instead, we speculated that the observed reactivity could be due to a ground-state preassembly of **[1-Co]**$^{2+}$ and NEt$_3$ prior to photoexcitation. Notably, similar explanations have been proposed for conPET and e-PRC reactions, and it has been demonstrated that such preassembly can exist even if it is not detectable by steady-state spectroscopic methods.[55,56] Indeed, while no significant change is observed in the UV/Vis-NIR absorption spectrum upon addition of NEt$_3$ to **[1-Co]**$^{2+}$, the excited-state lifetime of the ***[1-Co]**$^{2+}$ is decreased from 8 ps to 5 ps in the presence of NEt$_3$ (109 mM), consistent with this proposal (see section S6 in the SI). This corresponds to a rate constant of $7.5{\cdot}10^{10}$ s^{-1} for the PET process. Since no further intermediates were detected by transient absorption spectroscopy despite the reduction of the excited-state lifetime, we hypothesize that the geminate back electron transfer occurs significantly faster. This reduces the overall efficiency of the process (see also the discussion in section S6 in the SI).

The possibility of preassembly and potential charge-transfer pathways was also investigated computationally. First, the geometries of **[1-Co]**$^{2+}$ and **[1-Co]**$^+$ were optimized at the r^{2}SCAN–3c level of theory[57] using the ORCA[58–60] software package and verified as minima by the absence of imaginary vibrational frequencies. The calculated geometries of **[1-Co]**$^{2+}$ and **[1-Co]**$^+$ agree well with crystal data,[43] and selected bond lengths and angles are compiled in Tables S13 and S14 in the SI. Conformations of possible ground state assemblies between the starting species **[1-Co]**$^{2+}$ and NEt$_3$ were screened via metadynamics[61,62] at the semiempirical GFN2-xtb[63] level. 774 unique structures remained within an energy window of 2 kcal/mol above the lowest energy conformer, which will be considered as especially relevant in the following discussion of non-

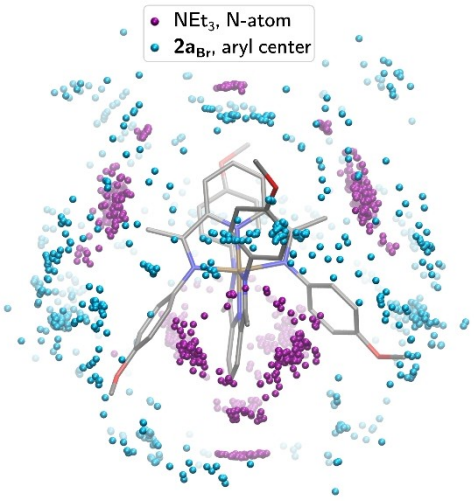

Figure 3. Visualization of the sampled (GFN2-xtb) preassemblies of **[1-Co]**$^{2+}$ with NEt_3 (purple) and **[1-Co]**$^{+}$ with 4-bromobenzonitrile (cyan) within an energy window of 2 kcal/mol of the lowest energy conformation. Colored spheres indicate the position of the coordinating N-atom (purple) or the center of the aryl unit (cyan) of the respective substrate. The coordination sites of the two substrates are complementary.

covalent preassemblies. Figure 3 reveals preferential coordination sites at the imine-bound methyl groups and at the pyridine units. In all cases, the bonding situation is best described as hydrogen bonds between the amine nitrogen and the ligand.

Six representative structures with NEt_3 coordinating to different positions of the complex were optimized with the higher-level r^{2}SCAN–3c method[57] to assess their thermodynamic stability (Table 1). Initial conditions for the geometry optimizations were selected manually to cover a wide range of possible binding sites. The formation of all optimized assemblies from the isolated molecules comes with a decrease in energy of 4.56–6.69 kcal/mol, which indicates that dispersive preassemblies are generally favorable in the ground state. Coordination at the axial positions of the pyridine units (b and f in Table 1), i.e., along the z-axis of the complex, is slightly less favorable than at other sites, which may be attributed to fewer possibilities for dispersive interactions between the amine and the catalyst at these positions. Apart from this, the energies of coordination to various positions around the complex are comparable.

Table 1: Energies and enthalpies for the formation of preassemblies between **[1-Co]**$^{n+}$ and substrates, relative to the energies of the isolated molecules (r^{2}SCAN–3c). Distances refer to the N–H distance for assemblies between **[1-Co]**$^{2+}$ and NEt_3, and to the center-to-center distance of interacting aromatic units for assemblies between **[1-Co]**$^{+}$ and $\mathbf{2a_{Br}}$ (see also Figures S54, S55, SI). Preassemblies with amines other than NEt_3 (g–k) are listed in Table S11, SI.

Cat.	Substr.	ID	ΔE [kcal/mol]	ΔH [kcal/mol]	Dist. [Å]
[1-Co]$^{2+}$	NEt_3	a	−6.69	−5.44	2.29
		b	−4.67	−3.52	2.38
		c	−6.44	−5.13	2.37
		d	−6.99	−5.59	2.59
		e	−6.61	−5.11	2.30
		f	−4.56	−3.35	2.32
[1-Co]$^{+}$	$2a_{Br}$	l	−7.94	−6.64	3.69
		m	−7.56	−6.38	4.85
		n	−8.36	−7.40	3.96
		o	−8.60	−7.26	4.10
		p	−8.20	−7.06	3.82
		q	−6.90	−5.80	3.54

Following the reduction of **[1-Co]**$^{2+}$ to **[1-Co]**$^{+}$, the possibility of preassembly with a model substrate for catalysis, 4-bromobenzonitrile ($\mathbf{2a_{Br}}$, Figure 3), revealed 826 conformations within 2 kcal/mol above the lowest energy structure. In this group, the dominant interaction among the lower-energy conformations is π-stacking between the 4-methoxyaniline units and the aromatic substrate. Toward higher energies, hydrogen bonds between ligand protons and the negatively polarized bromide become more prevalent. In contrast to NEt_3 coordination, the pyridine units of the ligand are excluded from the favorable coordination sites, which is attributed to the higher steric hindrance of the 4-bromobenzonitrile preventing π-stacking on these sites. Six structures were optimized (r^{2}SCAN–3c) and exhibit stabilization energies of 6.90–8.60 kcal/mol, compared to the isolated fragments. Out of these, three conformers (l, o and p in Table 1) are characterized by π-stacking interactions between one of the ligands and $\mathbf{2a_{Br}}$. In two cases (n and q), the substrate rather coordinates to one of the peripheral methoxy groups of the ligand, which are sterically more accessible than the aromatic units. The conformers n, o, and p are the most stable out of the optimized structures. Additionally, in one case (m), a T-π-interaction can be observed.

Comparing the two substrates, the favored coordination sites of NEt_3 and $\mathbf{2a_{Br}}$ appear complementary (Figure 3), indicating that both the amine and the substrate can in principle coordinate to the metal complex at the same time. To test this hypothesis, we sampled preassemblies with both NEt_3 and $\mathbf{2a_{Br}}$ coordinating simultaneously to either **[1-Co]**$^{2+}$ or **[1-Co]**$^{+}$. The results confirm the idea that both substrates have their preferred binding sites which are separate from each other (Figure S46, SI). As will be shown in the following sections, the photocatalytic mechanism likely consists of two consecutive steps. Therefore, simultaneous binding of both substrates to the catalyst is not a strict requirement for the electron transfer to occur. However, the two substrates not blocking each other's binding site is beneficial to the reaction, as it is less limited by the diffusion of the substrates. Thus, we conclude that both NEt_3 and $\mathbf{2a_{Br}}$ forming a stable dispersive assembly with the catalyst in the ground state enables the catalyst to efficiently mediate the electron transfer between the amine and the substrate $\mathbf{2a_{Br}}$.

Catalytic C–H arylation of N-methylpyrrole

The experimentally-proven feasibility of electron transfer from NEt_3 to *[**1-M**]$^{2+}$ and appropriate redox properties of the resulting **[1-M]**$^{+}$ imply that the salts **[1-M]**$(PF_6)_2$ should

be capable of mediating a full photocatalytic redox cycle. Thus, as a model reaction, the reductive coupling of aryl halides with pyrroles was investigated. This can be considered a "benchmark" reaction for the assessment of new **PC** candidates and has been studied for a variety of precious metal and organic catalysts.[64–77] However, to our knowledge there have been no previous reports of such C–H arylation reactions being successfully catalyzed by 3d metal complexes.

Initially, the coupling of 4-bromobenzonitrile $\mathbf{2a_{Br}}$ with *N*-methylpyrrole **3a** was targeted, and the results of this preliminary analysis are summarized in Table 2. Low catalyst loadings of both complexes **[1-M]**$(PF_6)_2$ (M=Fe, Co) promote the formation of the targeted cross-coupling product **4a** in good yield, alongside minor hydrodehalogenation of $\mathbf{2a_{Br}}$ to **5a** (for optimization studies, see SI). Control reactions confirmed that all reaction components are required.

Amines such as *N*,*N*-dimethylethylamine (DMEA), *N*,*N*-diisopropylethylamine (DIPEA) or diisopropylamine (DIPA) gave significantly lower yields of **4a** (see SI). When using the isostructural Ni and Zn complexes **[1-Ni]**$(PF_6)_2$ and **[1-Zn]**$(PF_6)_2$ significantly inferior results were obtained (see SI).[43] Under the best found conditions, both **[1-Fe]**$(PF_6)_2$ and **[1-Co]**$(PF_6)_2$ provided very good conversions of $\mathbf{2a_{Br}}$, but the highest yield of product **4a** was achieved using the Co complex, which is consistent with the easier photoinduced reduction by NEt_3 discussed above (although other factors such as the propensity of **[1-Fe]**(PF_6) for disproportionation may also be relevant). Accordingly, the reaction scope was explored employing **[1-Co]**$(PF_6)_2$ (Scheme 1; see the Supporting Information for the substrate scope of **[1-Fe]**$(PF_6)_2$). At optimized conditions, moderate to good yields of cross-coupling product can be obtained with electron-deficient aryl bromides. High yields up to 77 % are obtained with *p*-CN, *o*-CN, *o*-Br, and *p*-CF_3 substituents (products **4a**, **4b**, **4d**, and **4g**). In contrast, the *p*-Cl substituted product **4f** was obtained in a comparatively low yield of 36 %. Substrates with more electron-donating substituents resulted in lower activity, in line with previous reports using organic dyes such as rhodamine 6G and 4CzIPN.[67–77] Interestingly, the methodology is also suitable for aryl chlorides (albeit less efficiently), although they are

Table 2: Photoreductive coupling of 4-bromobenzonitrile $\mathbf{2a_{Br}}$ with *N*-methylpyrrole **3a** catalyzed by complexes **[1-M]**$(PF_6)_2$ (M=Fe, Co).

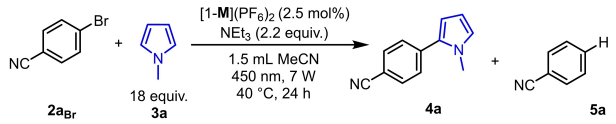

Entry	M	conversion $\mathbf{2a_{Br}}$ [%][a]	yield **4a** [%]	yield **5a** [%]
1	Fe	80	54	12
2	Co	90	77	12

[a] Conversion of starting material $\mathbf{2a_{Br}}$ as well as the yields of **4a** and the hydrodehalogenation product **5a** were determined by GC-FID using hexamethylbenzene as internal standard.

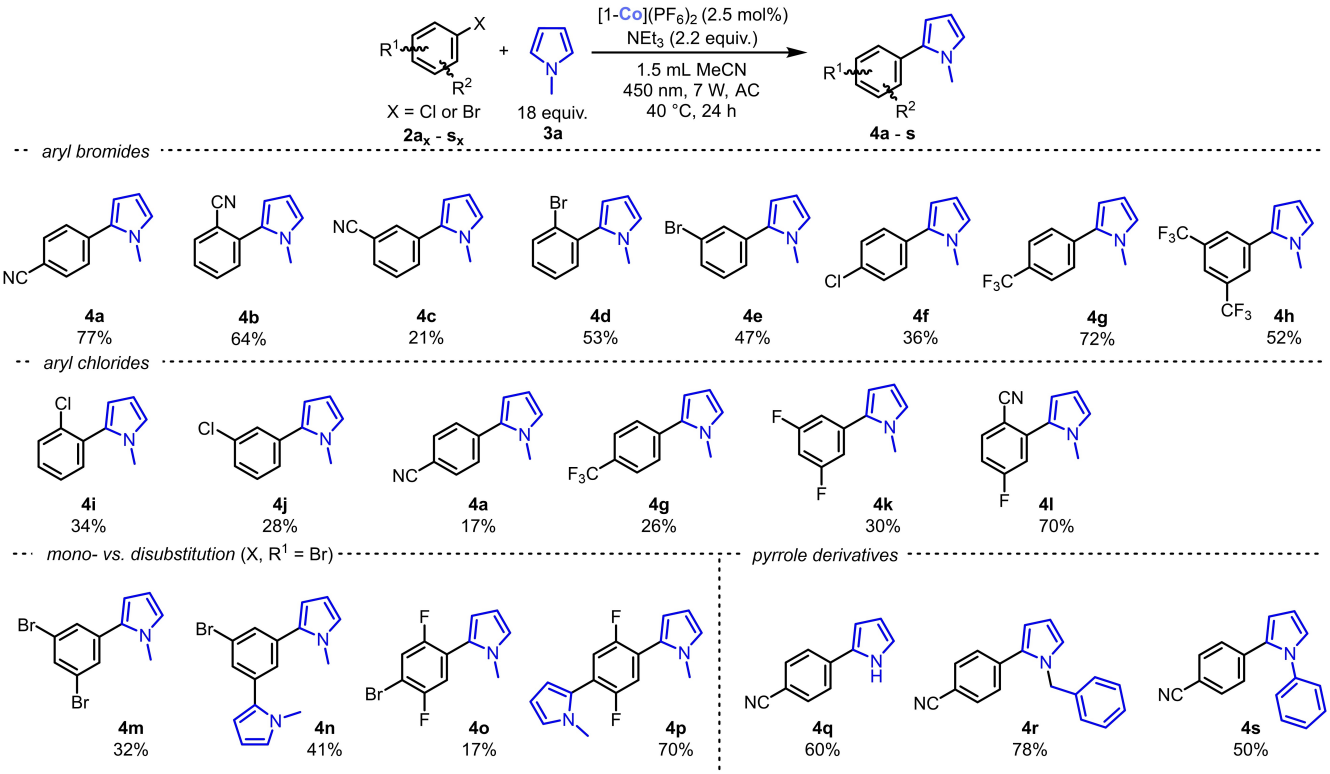

Scheme 1. Products **4a** to **4s** obtained by the light-driven C–H arylation reaction of pyrroles. Yields were obtained by GC-FID using hexamethylbenzene as internal standard. See the Supporting Information for the substrate scope of the analogous **[1-Fe]**$(PF_6)_2$.

typically considered very challenging to reduce (products **4i** to **4l**). For dibromoarenes, disubstitution was preferred over monosubstitution (cf. **4m** vs. **4n** and **4o** vs. **4p**), likely because the product of the latter is activated towards further functionalization.

Variation of the pyrrole coupling partner was also tolerated, and unsubstituted pyrrole, *N*-benzylpyrrole, and *N*-phenylpyrrole could all also be used to efficiently access the corresponding cross-coupled products (**4q** to **4s**). The results for **[1-Co]**$(PF_6)_2$ are comparable to the performance of organic dyes such as Rh-6G and 4CzIPN, while allowing for relatively low catalyst loadings and a facile work-up procedure.

Photoreactivity of [1-Co](PF$_6$)

Having already established the photoreactivity of **[1-Co]**$(PF_6)_2$ towards NEt_3, and confirmed in control experiments that it does not react with model substrates 4-bromobenzonitrile (**2a$_{Br}$**) or *N*-methylpyrrole (**3a**) in the absence of NEt_3 either under irradiation or in the dark (see SI), we sought to interrogate the reactivity of the reduced intermediate **[1-Co]**$^+$ in a similar manner. Irradiation of a solution containing all the components of the catalytic reaction, i.e., **[1-Co]**$(PF_6)_2$ (20 μM), NEt_3 (2 mM, 100 equiv.), 4-bromobenzonitrile (**2a$_{Br}$**, 6 mM, 300 equiv.), and *N*-methylpyrrole (**3a**, 10 mM, 500 equiv. with respect to **[1-Co]**$(PF_6)_2$ in MeCN (250 μL) (Figure S33, SI), with 405 nm light and monitoring by UV/Vis-NIR absorption spectroscopy showed initial formation of **[1-Co]**$^+$ (similarly to the results when using **[1-Co]**$(PF_6)_2$ and NEt_3 only, shown in Figure 2). However, further irradiation resulted in the total consumption of the initially formed **[1-Co]**$^+$ confirming that **[1-Co]**$^+$ is involved in subsequent reaction steps. Interestingly, when authentic, independently-prepared **[1-Co]**(PF_6) was combined with **2a$_{Br}$**, at catalytically relevant concentrations in THF oxidation of **[1-Co]**$^+$ to **[1-Co]**$^{2+}$ was observed by UV/Vis-NIR absorption spectroscopy upon irradiation at 405 nm (Figure 4).[78] These results suggest that, like **[1-Co]**$^{2+}$, **[1-Co]**$^+$ is also able to engage in electron transfer only upon photoexcitation, in this case being oxidized by **2a$_{Br}$**. It should be noted, however, that in contrast to the preceding reduction of **[1-Co]**$^{2+}$ (Figure 2, see above), in this case no defined isosbestic points were observed and the final spectrum, although similar, is not completely identical with that of pure **[1-Co]**$^{2+}$ (black dashed line in Figure 4a), indicating additional side reactions. Nevertheless, increasing the concentration of the substrate **2a$_{Br}$** significantly accelerated the oxidation of **[1-Co]**$^+$ (Figures S37 and S38, SI), while in the absence of substrate only a minor decrease of the **[1-Co]**$^+$ concentration was observed (Figure S36, SI), which is in agreement with the corresponding redox potentials (E_{red} (**2a$_{Br}$**) = −1.85 V vs. SCE;[79] $E_{1/2}$(**[1-Co]**$^{2+}$/**[1-Co]**$^+$) = −0.53 V vs. SCE) and provides evidence for a PET reaction between **[1-Co]**$^+$ and **2a$_{Br}$**.[43,79]

The PET reaction between **[1-Co]**$^+$ and **2a$_{Br}$** was also monitored by ^{1}H NMR spectroscopy (Figure 5). After

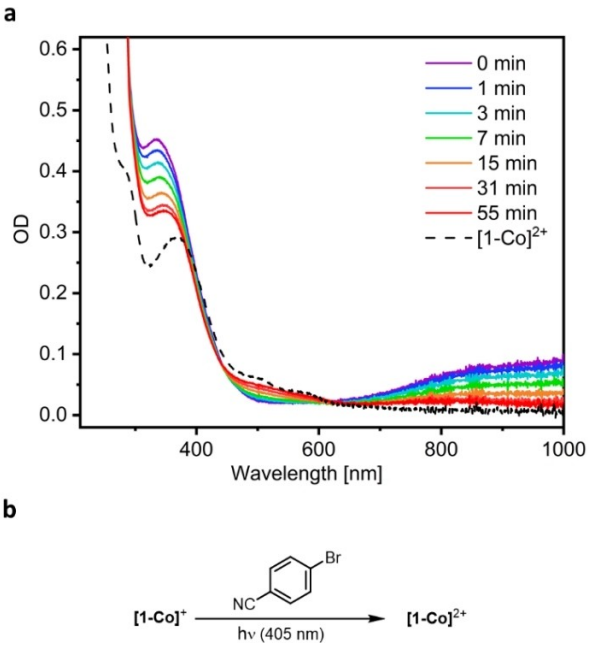

Figure 4. (a) Electronic absorption spectra in the UV/Vis-NIR spectral range of a mixture of **[1-Co]**(PF_6) (20 μM) and 4-bromobenzonitrile (**2a$_{Br}$**, 2000 μM) in THF (250 μL) after different intervals of irradiation at 405 nm. Black dashed line: Spectrum of **[1-Co]**$(PF_6)_2$ in THF for comparison. (b) Reaction equation for the observed photochemical reaction between **[1-Co]**$^+$ and **2a$_{Br}$**.

irradiation of **[1-Co]**$^+$ in the presence of 4-bromobenzonitrile (**2a$_{Br}$**, 1:1, 0.01 M in MeCN-d_3) for 2 h (450 nm, TAK120 AC photoreactor), the formation of **[1-Co]**$^{2+}$ is visible from the appearance of its characteristic, paramagnetically shifted ^{1}H NMR resonances (Figure 5d). An increase in the exposure time to 24 h results in partial decomposition of the complex, as indicated by new ^{1}H NMR signals at 36.7, 30.9, 26.4, 0.26, and −2.9 ppm (marked with an asterisk in Figure 5e, cf. a and d).

Electronic structure of [1-Co]$^{2+}$ and [1-Co]$^+$

To elucidate the electronic structure of the catalytic species, open-shell calculations on **[1-Co]**$^{2+}$ and **[1-Co]**$^+$ were performed once in the spin-unrestricted framework, which was also used for geometry optimizations, and once in a restricted open-shell formalism to eliminate spin-contamination. **[1-Co]**$^{2+}$ is best described as a low-spin Co^{2+} ion (d^7) coordinated by two neutral ligands, $[Co^{II}(L^0)_2]^{2+}$ (L = 2,6-bis[1-(4-methoxyphenylimino)ethyl]pyridine). The unpaired electron occupies the $d_{x^2-y^2}$ orbital and no significant spin density is observed on the ligands, even in the spin-unrestricted calculation (Figure S48, SI). Upon reduction to **[1-Co]**$^+$, the formerly unoccupied d_{z^2} orbital of the metal is populated, in agreement with previous experimental deductions.[43] However, a small amount of antiferromagnetic coupling between the metal ion and the ligand-based pyridine π-orbitals is observed for **[1-Co]**$^+$ in the spin-unrestricted calculation (S = 1.12, ideal: 1.00). Restricting the

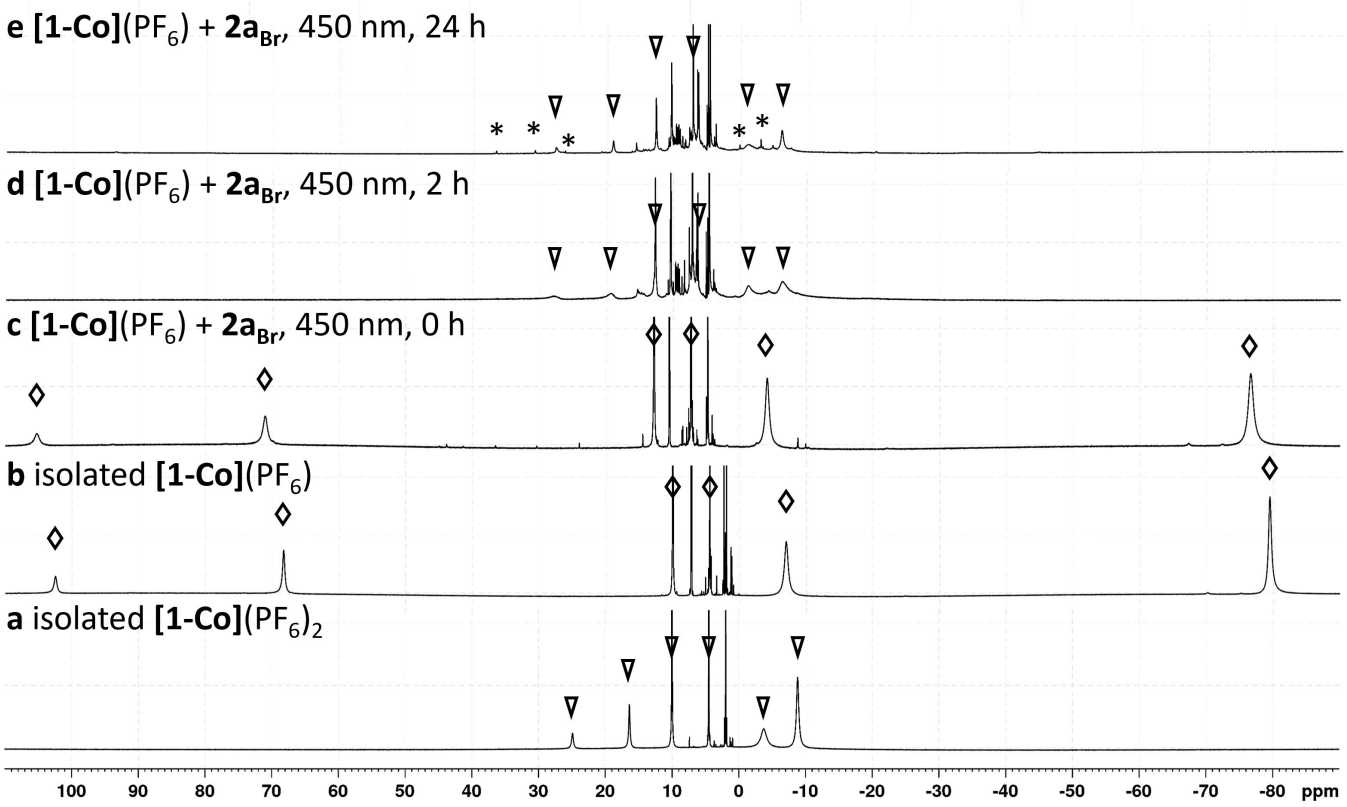

Figure 5. ^{1}H NMR spectra in MeCN-d_3 from bottom to top: (a) isolated **[1-Co]**$(PF_6)_2$, signals highlighted with ∇; (b) isolated **[1-Co]**(PF_6), signals highlighted with ; (c) isolated **[1-Co]**(PF_6) in presence of the substrate 4-bromobenzonitrile (**2a**$_{Br}$, 0.01 mM scale) before illumination; (d) isolated **[1-Co]**(PF_6) in presence of the substrate 4-bromobenzonitrile (**2a**$_{Br}$, 0.01 mM scale) after 2 h of illumination (TAK120 AC photoreactor, 7 W, 450 nm, 40 °C); (e) isolated **[1-Co]**(PF_6) in presence of the substrate 4-bromobenzonitrile (**2a**$_{Br}$, 0.01 mM scale) after 24 h of illumination (TAK120 AC photoreactor, 7 W, 450 nm, 40 °C), the signals of decomposition products are marked with an asterisk.

spin to a pure triplet leads to a rise in energy of 0.25 eV. The partial occupation of ligand orbitals in the ground state of **[1-Co]**$^+$ was further corroborated by CASSCF[80] and NEVPT2[81–83] calculations with the Molpro software package.[84–86] In particular, the d_{xz} and d_{yz} orbitals donate electron density into ligand-based π* orbitals, resulting in four partially occupied shells (Figure 6). Nevertheless, the triplet is favored over the quintet by an adiabatic energy difference of 0.4 eV (Table S12, SI). Therefore, the ground state of **[1-Co]**$^+$ is best described as a mixture of a Co^I ion coordinated by two neutral ligands ($[Co^I(L^0)_2]^+$) and a high-spin Co^{II} ion, coordinated by one neutral and one anionic ligand ($[Co^{II,HS}L^0L^-]^+$), setting the stage for subsequent electron transfer from the partially occupied π* orbitals.

Electron transfer mediated by [1-Co]$^{2+}$ and [1-Co]$^+$

To gain microscopic insight into the electron transfer processes, the absorption spectra for both the isolated complexes and the optimized catalyst-substrate aggregates were calculated. In a first step, the absorption properties of all optimized catalyst-substrate preassemblies were calculated at the low-cost r^{2}SCAN–3c level of theory in a TDA-DFT framework to assess the influence of the different preassembly conformations on the spectra. However, the energy of charge-transfer (CT) excitations is routinely underestimated in TD-DFT due to self-interaction errors.[87–91] Thus, higher-level calculations were performed at the TDA-SCS-ωPBEPP86/def2-TZVP(−f) level of theory for the complexes **[1-Co]**$^{2+}$ and **[1-Co]**$^+$ as well as for selected preassemblies. The range-separated double-hybrid density functional SCS-ωPBEPP86[92] includes a perturbative doubles correction and, thus, allows to describe CT excitations qualitatively.[90] Its use was crucial to reproduce the most prominent bands of the **[1-Co]**$^{2+}$ absorption spectrum (Figure 7). In general, the calculated spectrum of **[1-Co]**$^{2+}$ is blue-shifted with respect to the experimental spectrum. Therefore, an empirical correction of 0.65 eV was applied to all calculated energies in the following discussion. At low energies, the spectrum of **[1-Co]**$^{2+}$ is composed exclusively of dark d–d transitions. In the visible range, the spectrum features two distinct bands at 500 nm and 580 nm, calculated at 602 nm and 633 nm in Figure 7a, which arise from transitions to two MLCT states transferring electron density from the $d_{x^2-y^2}$ orbitals of the metal center to the pyridine units of either ligand. The prominent band with a maximum at 360 nm is dominated by ligand-centered π→π* transitions, mixed with transitions to ligand-to-ligand charge transfer (LLCT) states. The density of LLCT states

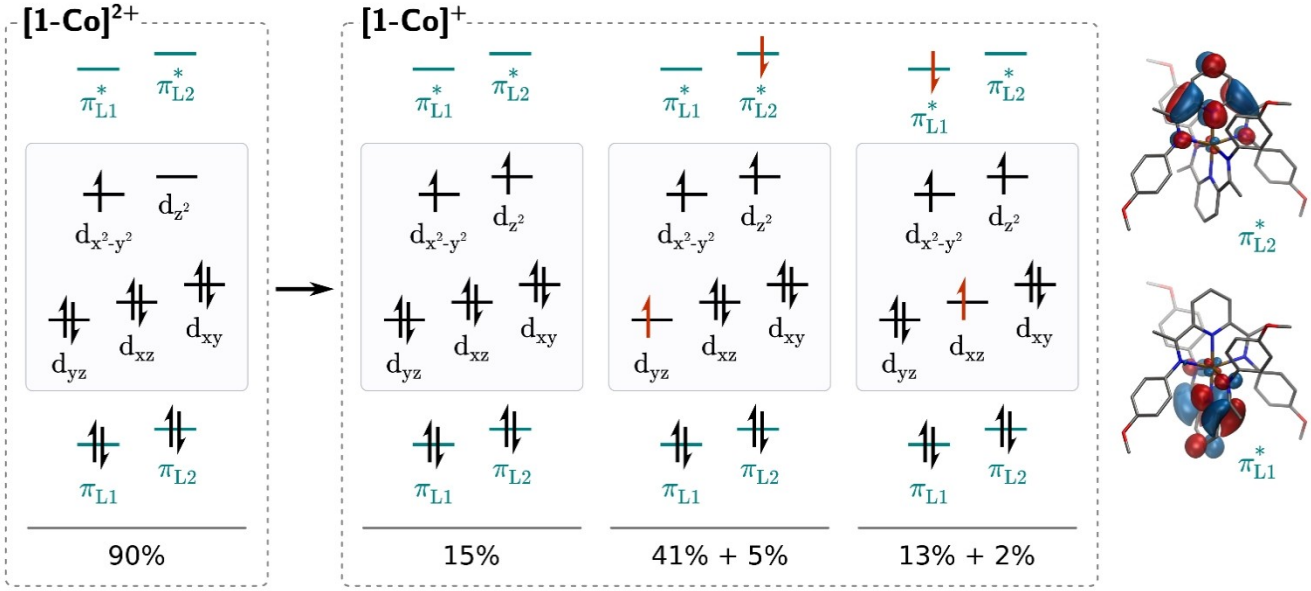

Figure 6. Leading configurations of the most stable ground-state wave function of **[1-Co]**$^{2+}$ and **[1-Co]**$^{+}$ at the CASSCF(12,9)/def2-TZVP level of theory. MO levels are plotted in energetic order but not to scale for clarity. Percentages indicate the weight of the respective configuration in the total CASSCF wave function. Split percentages refer to additional configurations, where the spins of the two electrons highlighted in red are reversed.

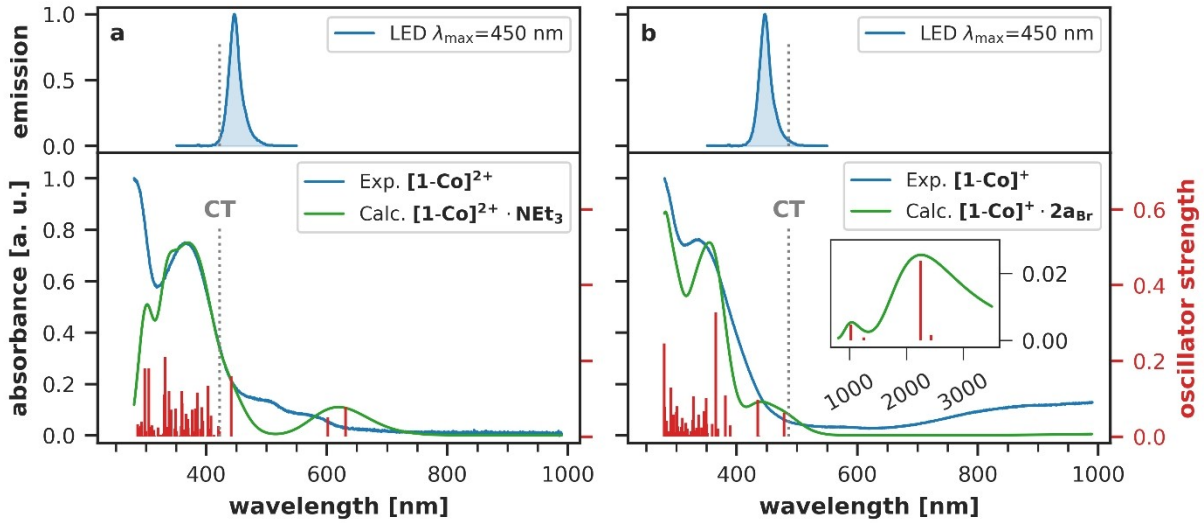

Figure 7. Calculated absorption spectra of representative preassemblies between (a) **[1-Co]**$^{2+}$ and NEt_3 and (b) **[1-Co]**$^{+}$ and $\mathbf{2a_{Br}}$ (TDA-SCS-ωPBEPP86/def2-TZVP(−f)), compared to experimental spectra of the complexes. A constant red-shift of 0.65 eV has been applied to the calculated spectrum (a); spectrum (b) has not been modified. In both cases, photoexcitation in the photoreactor occurs at $\lambda_{max} = 450$ nm. In this spectral region a CT state can be excited and transfer electron density (a) from the amine to **[1-Co]**$^{2+}$, forming **[1-Co]**$^{+}$, and subsequently (b) from **[1-Co]**$^{+}$ to $\mathbf{2a_{Br}}$. The inset in (b) illustrates excited states in the NIR region, which are red-shifted by the calculations compared to the experimental signal between 700 and 1000 nm.

increases towards higher energies. The dip in absorbance at 320 nm is explained by a higher density of excited states to which the transition from the ground state is of low probability.

Independent of the coordination site, aggregation of **[1-Co]**$^{2+}$ with NEt_3 introduces no distinct new spectral features (Figure S51, SI), in accordance with experimental observations (see the Supporting Information for details). Instead, in all of the investigated preassemblies a series of weak transitions to CT states is observed, in which electron density is transferred from the amine to the ligand. For one of the preassemblies (Figure 7a), the first such CT transition

(Figure 8a) appears at 422 nm, which is within the emission spectrum of the photoreactor LED, so that direct population of the $NEt_3 \rightarrow$ **[1-Co]**$^{2+}$ CT state is feasible, facilitating the reduction to **[1-Co]**$^{+}$. The low oscillator strength of this CT transition ($f = 0.0144$) is in qualitative accordance with the relatively long illumination times employed experimentally. Apart from direct excitation, the high density of states in this spectral region implies that the relevant CT state may also be populated via excited state dynamics, after excitation into a higher excited state.

The calculated spectrum for **[1-Co]**$^{+}$ agrees with the experimental data in the visible and UV range. The characteristic NIR band is shifted to lower energies by ~0.8 eV and consists of d–d transitions and intra-ligand $\pi \rightarrow \pi^*$ or LLCT excitations. This energy shift can be attributed to a higher degree of spin contamination in the ground state calculated at the SCS-ωPBEPP86 level ($<S^2> = 3.18$, ideal: 2.00) which leads to higher partial occupation of ligand π^* orbitals and thereby to lower excitation energies into these orbitals. This effect also compensates the previously observed blue-shift in the visible and UV range, such that no empirical correction is required for the calculated spectrum of **[1-Co]**$^{+}$. There are two bright excited states in the emission range of the photoreactor LED, one appearing at 480 nm, the other at 428 nm. They correspond to quasi-symmetry equivalent $\pi \rightarrow \pi^*$ excitations on one of the two pyridine units of the ligands. The absorption band at 340 nm is also dominated by ligand-centered $\pi \rightarrow \pi^*$ transitions. Toward higher energies, the absorbance first drops due to a series of weakly absorbing $\pi \rightarrow \pi^*$ and LLCT transitions, then rises again as the density of LLCT transitions increases. The spectrum of **[1-Co]**$^{+}$ remains largely unaffected by substrate coordination (Figure S51, SI), apart from additional UV bands due to substrate-based $\pi \rightarrow \pi^*$ excitations. In analogy to the oxidized species, the preassembly spectrum exhibits a weakly absorbing CT excitation (f = 0.0016) from the ligand to **2a**$_{Br}$ at 486 nm (Figure 8b), within the LED emission range. Excitation of this state effectively photo-reduces the substrate and thus enables the desired cleavage of the C–Br bond. The resulting hole on the ligand is filled by an electron from the metal upon returning to the ground state, restoring the original **[1-Co]**$^{2+}$ and completing the photocatalytic cycle.

Conceptualizing these insights, the ligand acts as an electron bridge between the redox-active metal and the other reactants. In the first photoactivated step, the ligand initially accepts an electron from the amine and transfers it partially over to the cobalt as the complex relaxes back to the ground state. Subsequently, excitation of the reduced complex transfers an electron from the ligand to the substrate, which causes the reoxidation of the metal upon deactivation. The electron transfer through the π^* orbitals (cf. Figure 6) of the diimininopyridine ligand is visually apparent in the calculated difference densities of the relevant CT states with respect to the ground state in the preassemblies (Figure 8).

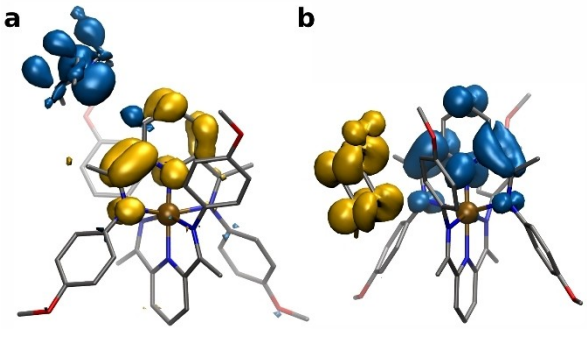

Figure 8. Difference densities of the relevant CT states with respect to the ground state in preassemblies between (a) **[1-Co]**$^{2+}$ and NEt_3 and (b) **[1-Co]**$^{+}$ and 4-bromobenzonitrile (**2a**$_{Br}$). Upon excitation, electron density is transferred from blue to yellow regions (isovalue: 0.002).

Mechanistic discussion

Based on the combined investigations described above, we propose the mechanism summarized in Scheme 2 for the **[1-Co]**$(PF_6)_2$-catalyzed arylation of **3a** by **2a**$_{Br}$. Interestingly, the presence of two separate PET steps implies that this can formally be considered as an example of conPET reactivity, which is more commonly associated with organic **PC**. This mechanism is initiated by preassembly between **[1-Co]**$^{2+}$ and the sacrificial electron donor NEt_3 (step i), which upon irradiation undergoes PET (step ii), yielding the one-electron reduction product **[1-Co]**$^{+}$. This can then engage in a second preassembly with the bromoarene **2a**$_{Br}$. After photoexcitation (step iii), **2a**$_{Br}$ is reduced to regenerate the initial **[1-Co]**$^{2+}$ (step iv). This PET process results in C–Br bond cleavage to afford the radical **2a**$^{\bullet}$, which can couple to

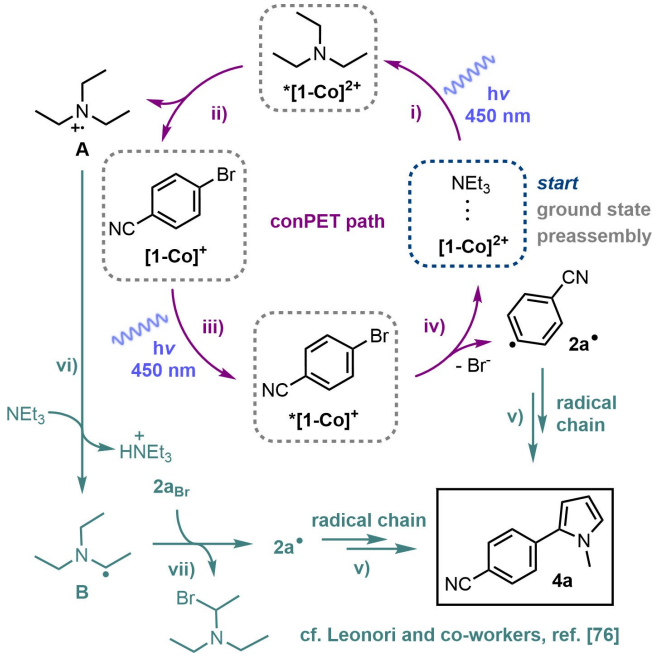

Scheme 2. Proposed mechanisms for the cobalt-catalyzed C– arylation of *N*-methylpyrrole.

N-methylpyrrole (step v), ultimately yielding product **4a** after further steps. For simplicity, these further steps are not shown in Scheme 2, but may include radical chain elements and/or re-reduction of $[\mathbf{1\text{-}Co}]^{2+}$ to $[\mathbf{1\text{-}Co}]^{+}$, as reported for other **PC**.[93] Note that an alternative mechanism based on Br atom transfer between $\mathbf{2a_{Br}}$ and the α-aminoalkyl radical **B** is also possible (Scheme 2, steps vi and vii; this has been proposed for organic **PC** such as 4CzIPN).[76,93] It is plausible that both pathways contribute to the C–H arylation reaction.[94] As illustrated in Scheme 2, NEt_3 fulfills several roles, acting as a reductant for photoexcited $*[\mathbf{1\text{-}Co}](PF_6)_2$, as a Brønsted base, and as a source of the radical **B**. Our quantum chemical calculations indicate that the preassembly of NEt_3 with $[\mathbf{1\text{-}Co}]^{2+}$ and the formation of radical **B** exhibit a favorable thermodynamic driving force (see Table S11 and Scheme S4, SI). This may explain the superior utility of NEt_3 over other amine bases (see above).

Conclusion

Despite a short excited-state lifetime, the readily accessible bis(diiminopyridine) cobalt complex $\mathbf{[1\text{-}Co]}(PF_6)_2$ is an efficient photocatalyst for the C–H arylation of pyrroles using both chloro- and bromoarenes as substrates. The performance of $\mathbf{[1\text{-}Co]}(PF_6)_2$ is comparable to that of precious metal-based complexes and organic dyes. Photoinduced electron transfer between the metal complex and the reactants is facilitated by preassembly processes and proceeds via the diiminopyridine ligands with intermediate metal oxidation. These results challenge the perception that the development of late 3d metal photocatalysts is dependent on the development of complexes with artificially extended excited-state lifetimes and suggests an alternative direction for the development of 3d-metal based PRC. While these results represent an important proof of concept, we believe that significant further improvements will be possible through ligand design, and that the insights reported herein will be applicable to a wide range of other PRC transformations. The application of $\mathbf{[1\text{-}Co]}(PF_6)_2$ and related metal complexes for a wider array of photochemical arylations is currently under investigation.

Supporting Information

The authors have cited additional references within the Supporting Information.[95–129]

Acknowledgements

The project was funded by the Deutsche Forschungsgemeinschaft (DFG, German Research Foundation)—TRR 325—444632635 (projects A4, A5 and C1). Open Access funding enabled and organized by Projekt DEAL.

Conflict of Interest

The authors declare no conflict of interest.

Data Availability Statement

The data that support the findings of this study are available in the supplementary material of this article. All optimized structures are provided as xyz files in a separate zip-Archive, available free of charge at https://doi.org/10.5281/zenodo.10528904.

Keywords: photoredox catalysis · cobalt · electron-transfer · arylation · quantum chemistry

[1] M. H. Shaw, J. Twilton, D. W. C. MacMillan, *J. Org. Chem.* **2016**, *81*, 6898–6926.
[2] L. Marzo, S. K. Pagire, O. Reiser, B. König, *Angew. Chem. Int. Ed.* **2018**, *57*, 10034–10072.
[3] R. C. McAtee, E. J. McClain, C. R. J. Stephenson, *Trends Chem.* **2019**, *1*, 111–125.
[4] P. Melchiorre, *Chem. Rev.* **2022**, *122*, 1483–1484.
[5] C. K. Prier, D. A. Rankic, D. W. C. MacMillan, *Chem. Rev.* **2013**, *113*, 5322–5363.
[6] N. A. Romero, D. A. Nicewicz, *Chem. Rev.* **2016**, *116*, 10075–10166.
[7] T. Duchanois, T. Etienne, C. Cebrián, L. Liu, A. Monari, M. Beley, X. Assfeld, S. Haacke, P. C. Gros, *Eur. J. Inorg. Chem.* **2015**, 2469–2477.
[8] L. Liu, T. Duchanois, T. Etienne, A. Monari, M. Beley, X. Assfeld, S. Haacke, P. C. Gros, *Phys. Chem. Chem. Phys.* **2016**, *18*, 12550–12556.
[9] A. Francés-Monerris, P. C. Gros, X. Assfeld, A. Monari, M. Pastore, *ChemPhotoChem* **2019**, *3*, 666–683.
[10] J. P. Zobel, O. S. Bokareva, P. Zimmer, C. Wölper, M. Bauer, L. González, *Inorg. Chem.* **2020**, *59*, 14666–14678.
[11] K. D. Vogiatzis, M. V. Polynski, J. K. Kirkland, J. Townsend, A. Hashemi, C. Liu, E. A. Pidko, *Chem. Rev.* **2019**, *119*, 2453–2523.
[12] D. M. Arias-Rotondo, J. K. McCusker, *Chem. Soc. Rev.* **2016**, *45*, 5803–5820.
[13] C. B. Larsen, O. S. Wenger, *Chem. Eur. J.* **2018**, *24*, 2039–2058.
[14] O. S. Wenger, *J. Am. Chem. Soc.* **2018**, *140*, 13522–13533.
[15] J. K. McCusker, *Science* **2019**, *363*, 484–488.
[16] B. M. Hockin, C. Li, N. Robertson, E. Zysman-Colman, *Catal. Sci. Technol.* **2019**, *9*, 889–915.
[17] S. Kaufhold, K. Wärnmark, *Catalysts* **2020**, *10*, 132.
[18] S. H. Kyne, G. Lefèvre, C. Ollivier, M. Petit, V.-A. R. Cladera, L. Fensterbank, *Chem. Soc. Rev.* **2020**, *49*, 8501–8542.
[19] A. Y. Chan, A. Ghosh, J. T. Yarranton, J. Twilton, J. Jin, D. M. Arias-Rotondo, H. A. Sakai, J. K. McCusker, D. W. C. MacMillan, *Science* **2023**, *382*, 191–197.
[20] R. Lauenstein, S. L. Mader, H. Derondeau, O. Z. Esezobor, M. Block, A. J. Römer, C. Jandl, E. Riedle, V. R. I. Kaila, J. Hauer, E. Thyrhaug, C. R. Hess, *Chem. Sci.* **2021**, *12*, 7521–7532.
[21] S. Paria, O. Reiser, *ChemCatChem* **2014**, *6*, 2477–2483.
[22] A. Hossain, A. Bhattacharyya, O. Reiser, *Science* **2019**, *364*, eaav9713.
[23] Y. Abderrazak, A. Bhattacharyya, O. Reiser, *Angew. Chem. Int. Ed.* **2021**, *60*, 21100–21115.

[24] M. Kaupp, *J. Comput. Chem.* **2007**, *28*, 320–325.
[25] K. Gadde, D. D. Vos, B. U. W. Maes, *Synthesis* **2023**, *55*, 164–192.
[26] L. Lindh, P. Chábera, N. W. Rosemann, J. Uhlig, K. Wärnmark, A. Yartsev, V. Sundström, P. Persson, *Catalysts* **2020**, *10*, 315.
[27] P. Chábera, Y. Liu, O. Prakash, E. Thyrhaug, A. E. Nahhas, A. Honarfar, S. Essén, L. A. Fredin, T. C. B. Harlang, K. S. Kjær, K. Handrup, F. Ericson, H. Tatsuno, K. Morgan, J. Schnadt, L. Häggström, T. Ericsson, A. Sobkowiak, S. Lidin, P. Huang, S. Styring, J. Uhlig, J. Bendix, R. Lomoth, V. Sundström, P. Persson, K. Wärnmark, *Nature* **2017**, *543*, 695–699.
[28] W. Leis, M. A. Argüello Cordero, S. Lochbrunner, H. Schubert, A. Berkefeld, *J. Am. Chem. Soc.* **2022**, *144*, 1169–1173.
[29] J. Moll, R. Naumann, L. Sorge, C. Förster, N. Gessner, L. Burkhardt, N. Ugur, P. Nuernberger, W. Seidel, C. Ramanan, M. Bauer, K. Heinze, *Chem. Eur. J.* **2022**, *28*, e202201858.
[30] J. P. Zobel, L. González, *JACS Au* **2021**, *1*, 1116–1140.
[31] P. Chábera, K. S. Kjaer, O. Prakash, A. Honarfar, Y. Liu, L. A. Fredin, T. C. B. Harlang, S. Lidin, J. Uhlig, V. Sundström, R. Lomoth, P. Persson, K. Wärnmark, *J. Phys. Chem. Lett.* **2018**, *9*, 459–463.
[32] A. Gualandi, M. Marchini, L. Mengozzi, M. Natali, M. Lucarini, P. Ceroni, P. G. Cozzi, *ACS Catal.* **2015**, *5*, 5927–5931.
[33] K. S. Kjær, N. Kaul, O. Prakash, P. Chábera, N. W. Rosemann, A. Honarfar, O. Gordivska, L. A. Fredin, K.-E. Bergquist, L. Häggström, T. Ericsson, L. Lindh, A. Yartsev, S. Styring, P. Huang, J. Uhlig, J. Bendix, D. Strand, V. Sundström, P. Persson, R. Lomoth, K. Wärnmark, *Science* **2018**, eaau7160.
[34] N. W. Rosemann, P. Chábera, O. Prakash, S. Kaufhold, K. Wärnmark, A. Yartsev, P. Persson, *J. Am. Chem. Soc.* **2020**, *142*, 8565–8569.
[35] A. Aydogan, R. E. Bangle, A. Cadranel, M. D. Turlington, D. T. Conroy, E. Cauët, M. L. Singleton, G. J. Meyer, R. N. Sampaio, B. Elias, L. Troian-Gautier, *J. Am. Chem. Soc.* **2021**, *143*, 15661–15673.
[36] A. Aydogan, R. E. Bangle, S. D. Kreijger, J. C. Dickenson, M. L. Singleton, E. Cauët, A. Cadranel, G. J. Meyer, B. Elias, R. N. Sampaio, L. Troian-Gautier, *Catal. Sci. Technol.* **2021**, *11*, 8037–8051.
[37] J. Schwarz, A. Ilic, C. Johnson, R. Lomoth, K. Wärnmark, *Chem. Commun.* **2022**, *58*, 5351–5354.
[38] J. Steube, A. Kruse, O. S. Bokareva, T. Reuter, S. Demeshko, R. Schoch, M. A. Argüello Cordero, A. Krishna, S. Hohloch, F. Meyer, K. Heinze, O. Kühn, S. Lochbrunner, M. Bauer, *Nat. Chem.* **2023**, *15*, 468–474.
[39] A. Ilic, J. Schwarz, C. Johnson, L. H. M. de Groot, S. Kaufhold, R. Lomoth, K. Wärnmark, *Chem. Sci.* **2022**, *13*, 9165–9175.
[40] A. K. Pal, C. Li, G. S. Hanan, E. Zysman-Colman, *Angew. Chem. Int. Ed.* **2018**, *57*, 8027–8031.
[41] S. Kaufhold, N. W. Rosemann, P. Chábera, L. Lindh, I. Bolaño Losada, J. Uhlig, T. Pascher, D. Strand, K. Wärnmark, A. Yartsev, P. Persson, *J. Am. Chem. Soc.* **2021**, *143*, 1307–1312.
[42] N. Sinha, B. Pfund, C. Wegeberg, A. Prescimone, O. S. Wenger, *J. Am. Chem. Soc.* **2022**, *144*, 9859–9873.
[43] B. de Bruin, E. Bill, E. Bothe, T. Weyhermüller, K. Wieghardt, *Inorg. Chem.* **2000**, *39*, 2936–2947.
[44] H. Huang, K. A. Steiniger, T. H. Lambert, *J. Am. Chem. Soc.* **2022**, *144*, 12567–12583.
[45] S. Wu, J. Kaur, T. A. Karl, X. Tian, J. P. Barham, *Angew. Chem. Int. Ed.* **2022**, *61*, e202107811.
[46] J. Castellanos-Soriano, J. C. Herrera-Luna, D. D. Díaz, M. C. Jiménez, R. Pérez-Ruiz, *Org. Chem. Front.* **2020**, *7*, 1709–1716.
[47] F. Glaser, C. Kerzig, O. S. Wenger, *Angew. Chem. Int. Ed.* **2020**, *59*, 10266–10284.
[48] J. P. Barham, B. König, *Angew. Chem. Int. Ed.* **2020**, *59*, 11732–11747.
[49] A. J. Rieth, M. I. Gonzalez, B. Kudisch, M. Nava, D. G. Nocera, *J. Am. Chem. Soc.* **2021**, *143*, 14352–14359.
[50] Y. Baek, A. Reinhold, L. Tian, P. D. Jeffrey, G. D. Scholes, R. R. Knowles, *J. Am. Chem. Soc.* **2023**, *145*, 12499–12508.
[51] S. J. Horsewill, G. Hierlmeier, Z. Farasat, J. P. Barham, D. J. Scott, *ACS Catal.* **2023**, *13*, 9392–9403.
[52] S. J. Horsewill, C. Cao, N. Dabney, E. S. Yang, S. Faulkner, D. J. Scott, *Chem. Commun.* **2023**, *59*, 14665–14668.
[53] M. H. Deniel, D. Lavabre, J. C. Micheau, in *Org. Photochromic Thermochromic Compd. Vol. 2 Physicochem. Stud. Biol. Appl. Thermochromism* (Eds.: J. C. Crano, R. J. Guglielmetti), Springer US, Boston, MA, **2002**, pp. 167–209.
[54] F. Brandl, S. Bergwinkl, C. Allacher, B. Dick, *Chem. Eur. J.* **2020**, *26*, 7946–7954.
[55] S. Wu, J. Žurauskas, M. Domański, P. S. Hitzfeld, V. Butera, D. J. Scott, J. Rehbein, A. Kumar, E. Thyrhaug, J. Hauer, J. P. Barham, *Org. Chem. Front.* **2021**, *8*, 1132–1142.
[56] A. Kumar, P. Malevich, L. Mewes, S. Wu, J. P. Barham, J. Hauer, *J. Chem. Phys.* **2023**, *158*, 144201.
[57] S. Grimme, A. Hansen, S. Ehlert, J.-M. Mewes, *J. Chem. Phys.* **2021**, *154*, 064103.
[58] F. Neese, *WIREs Comput. Mol. Sci.* **2012**, *2*, 73–78.
[59] F. Neese, F. Wennmohs, U. Becker, C. Riplinger, *J. Chem. Phys.* **2020**, *152*, 224108.
[60] F. Neese, *WIREs Comput. Mol. Sci.* **2022**, e1606.
[61] P. Pracht, F. Bohle, S. Grimme, *Phys. Chem. Chem. Phys.* **2020**, *22*, 7169–7192.
[62] S. Grimme, *J. Chem. Theory Comput.* **2019**, *15*, 2847–2862.
[63] C. Bannwarth, S. Ehlert, S. Grimme, *J. Chem. Theory Comput.* **2019**, *15*, 1652–1671.
[64] D. Alberico, M. E. Scott, M. Lautens, *Chem. Rev.* **2007**, *107*, 174–238.
[65] D. T. Gryko, O. Vakuliuk, D. Gryko, B. Koszarna, *J. Org. Chem.* **2009**, *74*, 9517–9520.
[66] M. Miura, T. Satoh, in *Modern Arylation Methods*, John Wiley & Sons, Ltd, **2009**, pp. 335–361.
[67] I. Ghosh, T. Ghosh, J. I. Bardagi, B. König, *Science* **2014**, *346*, 725–728.
[68] I. Ghosh, L. Marzo, A. Das, R. Shaikh, B. König, *Acc. Chem. Res.* **2016**, *49*, 1566–1577.
[69] I. Ghosh, B. König, *Angew. Chem. Int. Ed.* **2016**, *55*, 7676–7679.
[70] A. U. Meyer, T. Slanina, C.-J. Yao, B. König, *ACS Catal.* **2016**, *6*, 369–375.
[71] L. Marzo, I. Ghosh, F. Esteban, B. König, *ACS Catal.* **2016**, *6*, 6780–6784.
[72] I. Ghosh, R. S. Shaikh, B. König, *Angew. Chem. Int. Ed.* **2017**, *56*, 8544–8549.
[73] J. I. Bardagi, I. Ghosh, M. Schmalzbauer, T. Ghosh, B. König, *Eur. J. Org. Chem.* **2018**, 34–40.
[74] M. Neumeier, D. Sampedro, M. Májek, V. A. de la Peña O'Shea, A. Jacobi von Wangelin, R. Pérez-Ruiz, *Chem. Eur. J.* **2018**, *24*, 105–108.
[75] N. G. W. Cowper, C. P. Chernowsky, O. P. Williams, Z. K. Wickens, *J. Am. Chem. Soc.* **2020**, *142*, 2093–2099.
[76] T. Constantin, F. Juliá, N. S. Sheikh, D. Leonori, *Chem. Sci.* **2020**, *11*, 12822–12828.
[77] J. Wang, K. Schwedtmann, K. Liu, S. Schulz, J. Haberstroh, G. Schaper, A. Wenke, J. Naumann, T. Wenke, S. Wanke, J. J. Weigand, *Green Chem.* **2021**, *23*, 881–888.

[78] The experiments were performed in THF due to the higher photostability of **[1-Co]**$^+$ in that solvent. See the Supporting Information for further details (Figures S17, S18, S37 and S40).
[79] A. A. Isse, P. R. Mussini, A. Gennaro, *J. Phys. Chem. C* **2009**, *113*, 14983–14992.
[80] D. A. Kreplin, P. J. Knowles, H.-J. Werner, *J. Chem. Phys.* **2020**, *152*, 074102.
[81] C. Angeli, R. Cimiraglia, S. Evangelisti, T. Leininger, J.-P. Malrieu, *J. Chem. Phys.* **2001**, *114*, 10252–10264.
[82] C. Angeli, R. Cimiraglia, J.-P. Malrieu, *J. Chem. Phys.* **2002**, *117*, 9138–9153.
[83] C. Angeli, M. Pastore, R. Cimiraglia, *Theor. Chem. Acc.* **2007**, *117*, 743–754.
[84] H.-J. Werner, P. J. Knowles, G. Knizia, F. R. Manby, M. Schütz, *WIREs Comput. Mol. Sci.* **2012**, *2*, 242–253.
[85] H.-J. Werner, P. J. Knowles, F. R. Manby, J. A. Black, K. Doll, A. Heßelmann, D. Kats, A. Köhn, T. Korona, D. A. Kreplin, Q. Ma, T. F. Miller, A. Mitrushchenkov, K. A. Peterson, I. Polyak, G. Rauhut, M. Sibaev, *J. Chem. Phys.* **2020**, *152*, 144107.
[86] H.-J. Werner, P. J. Knowles, P. Celani, W. Györffy, A. Hesselmann, D. Kats, G. Knizia, A. Köhn, T. Korona, D. Kreplin, R. Lindh, Q. Ma, F. R. Manby, A. Mitrushenkov, G. Rauhut, M. Schütz, K. R. Shamasundar, T. B. Adler, R. D. Amos, S. J. Bennie, A. Bernhardsson, A. Berning, J. A. Black, P. J. Bygrave, R. Cimiraglia, D. L. Cooper, D. Coughtrie, M. J. O. Deegan, A. J. Dobbyn, K. Doll, M. Dornbach, F. Eckert, S. Erfort, E. Goll, C. Hampel, G. Hetzer, J. G. Hill, M. Hodges, T. Hrenar, G. Jansen, C. Köppl, C. Kollmar, S. J. R. Lee, Y. Liu, A. W. Lloyd, R. A. Mata, A. J. May, B. Mussard, S. J. McNicholas, W. Meyer, T. F. Miller III, M. E. Mura, A. Nicklass, D. P. O'Neill, P. Palmieri, D. Peng, K. A. Peterson, K. Pflüger, R. Pitzer, I. Polyak, M. Reiher, J. O. Richardson, J. B. Robinson, B. Schröder, M. Schwilk, T. Shiozaki, M. Sibaev, H. Stoll, A. J. Stone, R. Tarroni, T. Thorsteinsson, J. Toulouse, M. Wang, M. Welborn, B. Ziegler, *MOLPRO*, *Version 2023.2,a Package of Ab Initio Programs*, **2023**.
[87] S. Grimme, M. Parac, *ChemPhysChem* **2003**, *4*, 292–295.
[88] A. Dreuw, M. Head-Gordon, *J. Am. Chem. Soc.* **2004**, *126*, 4007–4016.
[89] M. Campetella, F. Maschietto, M. J. Frisch, G. Scalmani, I. Ciofini, C. Adamo, *J. Comput. Chem.* **2017**, *38*, 2151–2156.
[90] D. Mester, M. Kállay, *J. Chem. Theory Comput.* **2022**, *18*, 1646–1662.
[91] J. P. Zobel, A. Kruse, O. Baig, S. Lochbrunner, S. I. Bokarev, O. Kühn, L. González, O. S. Bokareva, *Chem. Sci.* **2023**, *14*, 1491–1502.
[92] M. Casanova-Páez, L. Goerigk, *J. Chem. Theory Comput.* **2021**, *17*, 5165–5186.
[93] T. Constantin, M. Zanini, A. Regni, N. S. Sheikh, F. Juliá, D. Leonori, *Science* **2020**, *367*, 1021–1026.
[94] This mechanism is consistent with the calculated thermodynamics for the deprotonation of the triethylamine radical cation **A** (Scheme , step vi) to generate **B** and the subsequent oxidation of **B** by $\mathbf{2}_{\mathbf{aBr}}$ (step vii; see the Supporting Information for details).
[95] B. L. Small, M. Brookhart, A. M. A. Bennett, *J. Am. Chem. Soc.* **1998**, *120*, 4049–4050.
[96] A. L. Vance, N. W. Alcock, J. A. Heppert, D. H. Busch, *Inorg. Chem.* **1998**, *37*, 6912–6920.
[97] G. M. Duarte, J. D. Braun, P. K. Giesbrecht, D. E. Herbert, *Dalton Trans.* **2017**, *46*, 16439–16445.
[98] Z.-J. Li, S. Li, E. Hofman, A. H. Davis, G. Leem, W. Zheng, *Green Chem.* **2020**, *22*, 1911–1918.
[99] R. J. Kutta, N. Archipowa, N. S. Scrutton, *Phys. Chem. Chem. Phys.* **2018**, *20*, 28767–28776.
[100] T. Pavlovska, D. Král Lesný, E. Svobodová, I. Hoskovcová, N. Archipowa, R. J. Kutta, R. Cibulka, *Chem. Eur. J.* **2022**, *28*, e202200768.
[101] E. Caldeweyher, S. Ehlert, A. Hansen, H. Neugebauer, S. Spicher, C. Bannwarth, S. Grimme, *J. Chem. Phys.* **2019**, *150*, 154122.
[102] H. Kruse, S. Grimme, *J. Chem. Phys.* **2012**, *136*, 154101.
[103] M. Cossi, N. Rega, G. Scalmani, V. Barone, *J. Comput. Chem.* **2003**, *24*, 669–681.
[104] S. Grimme, *Chem. Eur. J.* **2012**, *18*, 9955–9964.
[105] Y. Guo, C. Riplinger, U. Becker, D. G. Liakos, Y. Minenkov, L. Cavallo, F. Neese, *J. Chem. Phys.* **2018**, *148*, 011101.
[106] Y. Guo, C. Riplinger, D. G. Liakos, U. Becker, M. Saitow, F. Neese, *J. Chem. Phys.* **2020**, *152*, 024116.
[107] D. G. Liakos, Y. Guo, F. Neese, *J. Phys. Chem. A* **2020**, *124*, 90–100.
[108] E. van Lenthe, E. J. Baerends, J. G. Snijders, *J. Chem. Phys.* **1993**, *99*, 4597–4610.
[109] C. van Wüllen, *J. Chem. Phys.* **1998**, *109*, 392–399.
[110] F. Weigend, R. Ahlrichs, *Phys. Chem. Chem. Phys.* **2005**, *7*, 3297–3305.
[111] J. Zheng, X. Xu, D. G. Truhlar, *Theor. Chem. Acc.* **2011**, *128*, 295–305.
[112] F. Neese, F. Wennmohs, A. Hansen, U. Becker, *Chem. Phys.* **2009**, *356*, 98–109.
[113] R. Izsák, F. Neese, *J. Chem. Phys.* **2011**, *135*, 144105.
[114] S. Kossmann, F. Neese, *Chem. Phys. Lett.* **2009**, *481*, 240–243.
[115] A. Hellweg, C. Hättig, S. Höfener, W. Klopper, *Theor. Chem. Acc.* **2007**, *117*, 587–597.
[116] F. Weigend, *Phys. Chem. Chem. Phys.* **2006**, *8*, 1057–1065.
[117] W. Humphrey, A. Dalke, K. Schulten, *J. Mol. Graphics* **1996**, *14*, 33–38.
[118] F. Neese, *J. Phys. Chem. Solids* **2004**, *65*, 781–785.
[119] F. Weigend, *J. Comput. Chem.* **2008**, *29*, 167–175.
[120] J. P. Perdew, *Phys. Rev. B* **1986**, *33*, 8822–8824.
[121] J. P. Perdew, *Phys. Rev. B* **1986**, *34*, 7406–7406.
[122] A. D. Becke, *Phys. Rev. A* **1988**, *38*, 3098–3100.
[123] S. Grimme, J. Antony, S. Ehrlich, H. Krieg, *J. Chem. Phys.* **2010**, *132*, 154104.
[124] S. Grimme, S. Ehrlich, L. Goerigk, *J. Comput. Chem.* **2011**, *32*, 1456–1465.
[125] S. Hirata, M. Head-Gordon, *Chem. Phys. Lett.* **1999**, *314*, 291–299.
[126] F. Plasser, *J. Chem. Phys.* **2020**, *152*, 084108.
[127] F. Plasser, M. Wormit, A. Dreuw, *J. Chem. Phys.* **2014**, *141*, 024106.
[128] F. Plasser, H. Lischka, *J. Chem. Theory Comput.* **2012**, *8*, 2777–2789.
[129] T. J. Lee, P. R. Taylor, *Int. J. Quantum Chem.* **1989**, *36*, 199–207.

Manuscript received: March 25, 2024
Accepted manuscript online: May 1, 2024